

Improving qubit coherence using closed-loop feedback

Antti Vepsäläinen,^{1,*} Roni Winik,¹ Amir H. Karamlou,^{2,1} Jochen Braumüller,¹ Agustin Di Paolo,¹ Youngkyu Sung,² Bharath Kannan,² Morten Kjaergaard,^{1,3} David K. Kim,⁴ Alexander J. Melville,⁴ Bethany M. Niedzielski,⁴ Jonilyn L. Yoder,⁴ Simon Gustavsson,¹ and William D. Oliver^{2,4}

¹*Research Laboratory of Electronics, Massachusetts Institute of Technology*

²*Department of Electrical Engineering and Computer Science, Massachusetts Institute of Technology*

³*Center for Quantum Devices, University of Copenhagen*

⁴*MIT Lincoln Laboratory*

(Dated: January 7, 2022)

Superconducting qubits are a promising platform for building a larger-scale quantum processor capable of solving otherwise intractable problems. In order for the processor to reach practical viability, the gate errors need to be further suppressed and remain stable for extended periods of time. With recent advances in qubit control, both single- and two-qubit gate fidelities are now in many cases limited by the coherence times of the qubits. Here we experimentally employ closed-loop feedback to stabilize the frequency fluctuations of a superconducting transmon qubit, thereby increasing its coherence time by 26% and reducing the single-qubit error rate from $(8.5 \pm 2.1) \times 10^{-4}$ to $(5.9 \pm 0.7) \times 10^{-4}$. Importantly, the resulting high-fidelity operation remains effective even away from the qubit flux-noise insensitive point, significantly increasing the frequency bandwidth over which the qubit can be operated with high fidelity. This approach is helpful in large qubit grids, where frequency crowding and parasitic interactions between the qubits limit their performance.

I. INTRODUCTION

High fidelity single- and two-qubit gates are a prerequisite for high-depth circuits and quantum error correction. For many qubit modalities, including superconducting qubits, the qubit frequencies and their controls are subject to temporally correlated noise - most notably $1/f$ -type noise - resulting in correlated errors and slow drifts in frequency. Here, we use active feedback control to stabilize the frequency drift of a flux-tunable superconducting transmon qubit and thereby suppress its temporal frequency fluctuations. This results in improved coherence times and gate fidelities, which remain stable over extended periods of time.

Closed-loop feedback control is ubiquitously used in a wide variety of engineering applications. There is an increasing number of experiments where feedback is used to modify the evolution of quantum systems, such as stabilizing the motion of the atoms in optical cavities [1], cooling quantum mechanical resonators [2], or stabilizing Rabi oscillations in superconducting qubits [3]. These experiments are based on continuous monitoring of the system, which inevitably decoheres the quantum state. In Ref. [4], a method based on interleaving the probing sequences with separate periods of time used for computation was introduced and demonstrated to mitigate the effect of slow magnetic field fluctuations. In Ref. [5], it was further shown that this method can be used to decouple an electron spin from low frequency magnetic field fluctuations, resulting in improved coherence times. Ref. [6] employs a slightly different approach in a trapped-ion system, where spectator qubits are used to

probe spatially correlated errors in the control laser amplitude and targeting. Here, we demonstrate that closed-loop feedback can be used to mitigate decoherence and improve gate fidelities in a frequency-tunable superconducting qubit system.

The dominant source of decoherence in superconducting qubits is typically either charge noise or flux noise but depending on the qubit design also photon shot noise [7] or Bogoliubov quasiparticles may contribute [8]. These noise sources are primarily intrinsic and local to the device [9, 10] — as opposed to noise in the control electronics — though recently there has been some evidence of correlated noise between the qubits [11–13]. In our experiment, we employ flux-tunable transmon qubits [14], which are widely used in contemporary superconducting quantum processors [15, 16]. Due to their design, transmons are mostly insensitive to charge-noise [14], but suffer from noise in magnetic flux, which is used to tune their frequency. In order to protect the qubits from flux noise, these qubits are typically operated at bias points where their frequency is first-order insensitive to small changes in flux, colloquially referred to as a sweet spot, see Fig. 1a. However, in many architectures the qubits cannot be operated at the sweet spot indefinitely while performing logic operations [17, 18]. Additionally, it is necessary to operate some of the qubits away from their sweet spots, in part due to parasitic couplings to two-level fluctuators with frequencies near the sweet spot [19–22] or couplings to other qubits or their higher excited states in the quantum processor [16]. We demonstrate that using the feedback protocol to suppress low frequency noise enables gate fidelities exceeding 99.9% even far away from the flux sweet spot, greatly extending the range of available operation frequencies for such qubits.

* avepsala@mit.edu

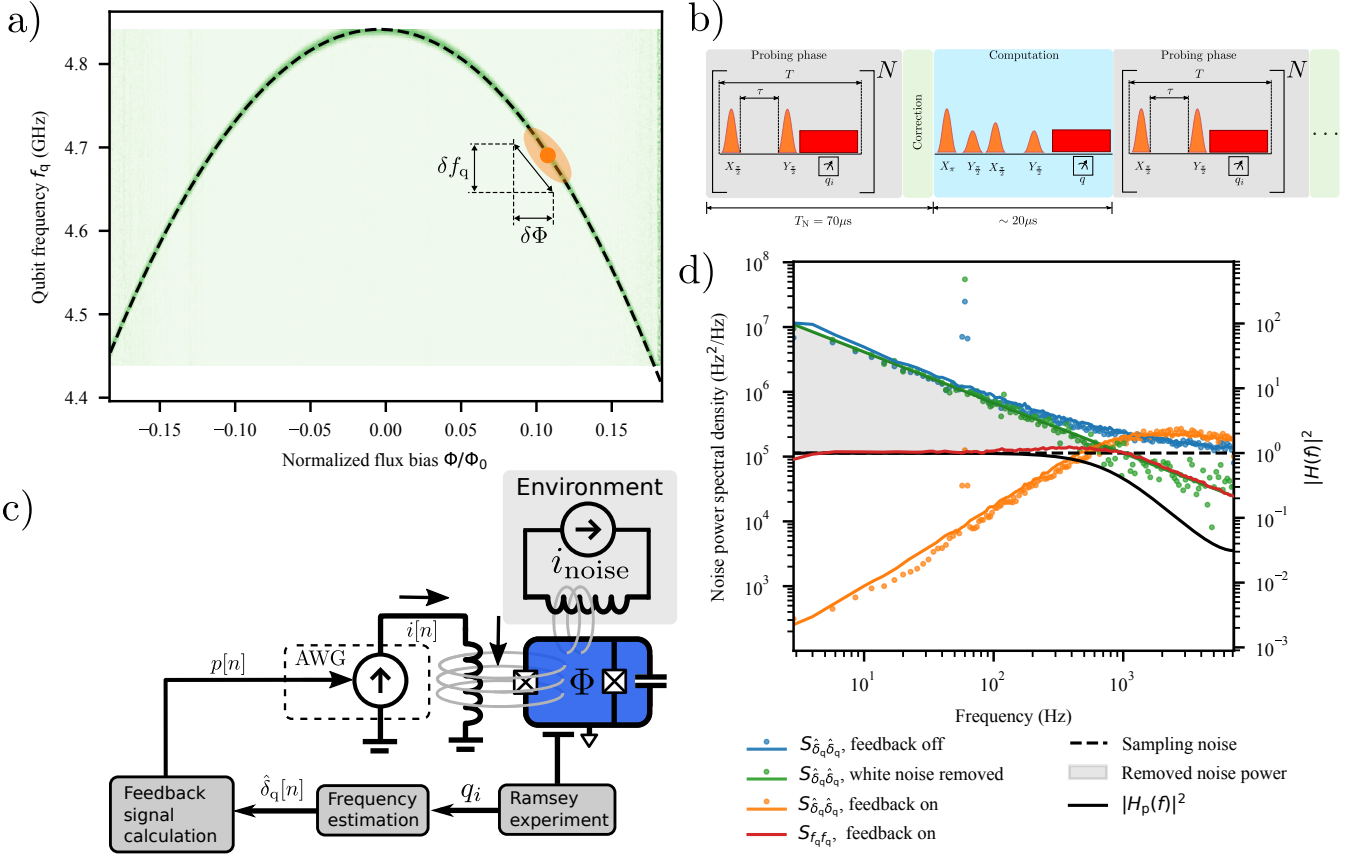


FIG. 1. **Qubit frequency power spectral density** a) The spectrum of the qubit as a function of flux bias. The orange dot shows the flux bias point at which the qubit is operated. b) Schematic of the frequency estimation pulse sequence (grey) interleaved with the sequence used for computation (light blue). The qubit frequency is adjusted in between (green). c) Schematic of the feedback loop. The measurement record q_i of a repeated Ramsey experiment is used to estimate the qubit frequency offset $\hat{\delta}_q[n]$ subject to a noisy environment i_{noise} . The feedback signal $p[n]$ controls an AWG that produces a current $i[n]$ to cancel the fluctuations in the qubit frequency. d) Power spectral density of the qubit frequency fluctuations estimated from $N = 20$ Ramsey experiments $S_{\delta_q \delta_q}(f)$, limited by the statistical sampling noise (dashed black line). The spectrum with the sampling noise suppressed using cross-correlation between consecutive samples is shown with green dots along with a fit (green line). Orange dots (line) are the measured (simulated) power spectral density of the error signal $\hat{\delta}_q[n]$ with the feedback activated. The simulated power spectral density of the actual qubit frequency fluctuations $f_q(t)$ is shown with solid red line. The gray background describes the noise power removed by the feedback. The frequency response of the feedback signal is overlaid in the plot with solid black line.

II. RESULTS

The feedback protocol we employ consists of three phases that are continuously repeated, see Fig 1b. In the probing phase, the qubit frequency is estimated using a simple single-qubit frequency estimation algorithm. After the frequency of the qubit is estimated, the magnetic flux through the qubit SQUID loop is adjusted to set the qubit frequency to its target value. This is followed by a computation phase, where an algorithm can be run with a freshly stabilized qubit.

The probing phase consists of N repeated Ramsey measurements. For each of those measurements, the qubit is first prepared in a superposition state $|\psi\rangle = (|0\rangle + |1\rangle)/\sqrt{2}$ using a $\pi/2$ rotation around the y -axis

of the Bloch sphere. The state preparation is followed by a period of free evolution for a duration τ , during which the qubit state acquires a phase $\phi = 2\pi \int_0^\tau \delta_q(t) dt$, where $\delta_q(t) = f_d - f_q(t)$ is the detuning between a microwave drive frequency f_d defining a rotating reference frame, and $f_q(t)$ is the fluctuating qubit frequency in the presence of noise. A second $\pi/2$ pulse is then applied around the x -axis, and the state of the qubit is measured using dispersive readout [23]. To simplify the feedback protocol, we make a quasi-static approximation and assume that the qubit frequency remains constant within one frequency estimation experiment – N Ramsey measurements – but may fluctuate between the experiments. With this assumption, the probability of measuring the

qubit in the excited state is given by

$$p_1 = \frac{1}{2} + \frac{1}{2} \cos(2\pi\delta_q\tau - \pi/2), \quad (1)$$

which can be inverted to yield the frequency shift

$$\delta_q = \frac{\pm \arccos(2p_1 - 1) + 2\pi k + \pi/2}{2\pi\tau}, \quad (2)$$

where k is an integer. Equation (2) is a one-to-one mapping from p_1 to the frequency detuning δ_q over the domain $\delta_q \in [-\frac{1}{4\tau}, \frac{1}{4\tau}]$. This implies the fluctuations in δ_q need to be within $\pm \frac{1}{4\tau}$ between the estimation steps, approximately 70 μ s in our experiment.

The qubit excited-state probability estimator $\hat{p}_1 = \frac{1}{N} \sum_{i=0}^N q_i$ is calculated from the measurement record q_i of $N = 20$ repetitions of the Ramsey sequence, providing an estimate for the frequency detuning of the qubit, $\hat{\delta}_q$. If in the previous measurement the qubit was measured to be in the excited state, we virtually reset the qubit state for the current repetition by flipping q_i [24, 25]. The duration of a Ramsey measurement is $T = 3.5 \mu$ s, comprising the phase accumulation time $\tau = 1.25 \mu$ s, the readout duration of 750 ns, and the combined resonator reset time and overhead from the electronics, 1.5 μ s. Thus, a single round of frequency estimation takes $T_N = NT = 70 \mu$ s in our implementation. The frequency estimation is not able to detect fluctuations that occur faster than the repetition period of the feedback, ultimately limiting the effective bandwidth of the noise suppression. Next we investigate how the feedback reduces the noise spectral density of the qubit.

A. Noise spectral density

To estimate the noise power spectral density affecting the qubit frequency, we first bias the qubit away from the sweet spot by 0.11 flux quanta $\Phi_0 = h/2e$, at a transition frequency $f_q = 4.69$ GHz that is sensitive to flux noise (Fig. 1a), and repeatedly estimate its frequency 10^5 times. The blue dots in Fig. 1d show the power spectral density of the measured qubit frequency fluctuations subject to flux noise. The measured power spectral density follows a power law (green solid line) $S_{f_q f_q}(f) = A_{f_q} \left(\frac{1 \text{ Hz}}{f}\right)^\alpha \approx 27.3 \times 10^6 \text{ Hz}^2/\text{Hz} \times \left(\frac{1 \text{ Hz}}{f}\right)^{0.8}$, but starts to deviate at frequencies above 500 Hz for $N = 20$ and $\tau = 1.25 \mu$ s. This is due to noise added by the finite number of samples in the estimate $\hat{\delta}_q$ and can be approximated as

$$\delta\hat{\delta}_q \approx \frac{1}{2\pi\tau\sqrt{N}}, \quad (3)$$

see Supplementary material for the derivation. The statistical sampling noise is modeled as Gaussian white noise

with an upper cutoff given by the duration of the frequency estimation [26],

$$S_{\text{est}}(f) = \begin{cases} \frac{T}{2\pi^2\tau^2}, & 0 \leq f \leq \frac{1}{2NT}, \\ 0, & \text{otherwise,} \end{cases} \quad (4)$$

shown with dashed black line in Fig. 1d. The sampling noise can be suppressed in post-processing by cross-correlating time-shifted measurement traces as demonstrated in Ref. [26]. The results of applying this protocol are shown with green dots in Fig. 1d. With the sampling noise suppressed, the measured power spectrum fits well to the power law across the whole bandwidth. There is an additional peak at 60 Hz corresponding to the noise from the mains power. The sampling noise suppression is not used in the real-time feedback signal calculation due to small amount of samples available at the time of computation.

Next, we turn on the feedback to reduce the fluctuations in the qubit frequency. We aim to minimize the deviation of the qubit frequency $f_q(t)$ from the target frequency f_d by using the offset $\hat{\delta}_q[n]$ as the error signal in the feedback loop, see Fig. 1c for the schematic of the signal flow. Here we use n to number each time feedback is applied, sampled at times $t_n = nT_N$. In practice, the sampled error signal represents the average of the qubit frequency fluctuation during the sampling period T_N , limiting the maximum bandwidth of the feedback to $1/(2T_N) \approx 7$ kHz if the time spent on the interleaved computation step is omitted. The error signal $\hat{\delta}_q[n]$ is multiplied by a controllable gain G and fed into an accumulator that controls the feedback signal, $p[n] = p[n-1] + G\hat{\delta}_q[n]$. We deliberately set $G = 0.35$ to reduce the bandwidth of the feedback frequency response $H_p(f)$, shown with solid black line in Fig. 1d, to be less affected by the statistical sampling noise, see Supplementary material for additional details.

The output of the accumulator $p[n]$ is scaled and converted to an arbitrary waveform generator voltage that drives the current responsible for creating a magnetic flux through the qubit loop, adjusting its transition frequency. The feedback significantly reduces the noise spectral density of the error-signal $\hat{\delta}_q[n]$, shown with orange dots in Fig. 1d.

After closing the feedback loop, the error signal $\hat{\delta}_q[n]$ provides only indirect information about the actual qubit frequency fluctuations, which are also affected by the frequency response of the feedback (see Supplementary material for theoretical analysis). Thereby, we employ a simulation to assess the impact of the feedback transfer function on stabilizing the qubit frequency $f_q(t)$. We use the fitted noise spectral density as the starting point of the simulation (green solid line in Fig. 1d) to generate time traces of the fluctuating qubit frequencies. Using the same parameters as in the experiment, we simulate the estimation of the qubit frequency and the feedback, which results in a time trace of estimated qubit frequencies. The power spectral density of the simulated qubit

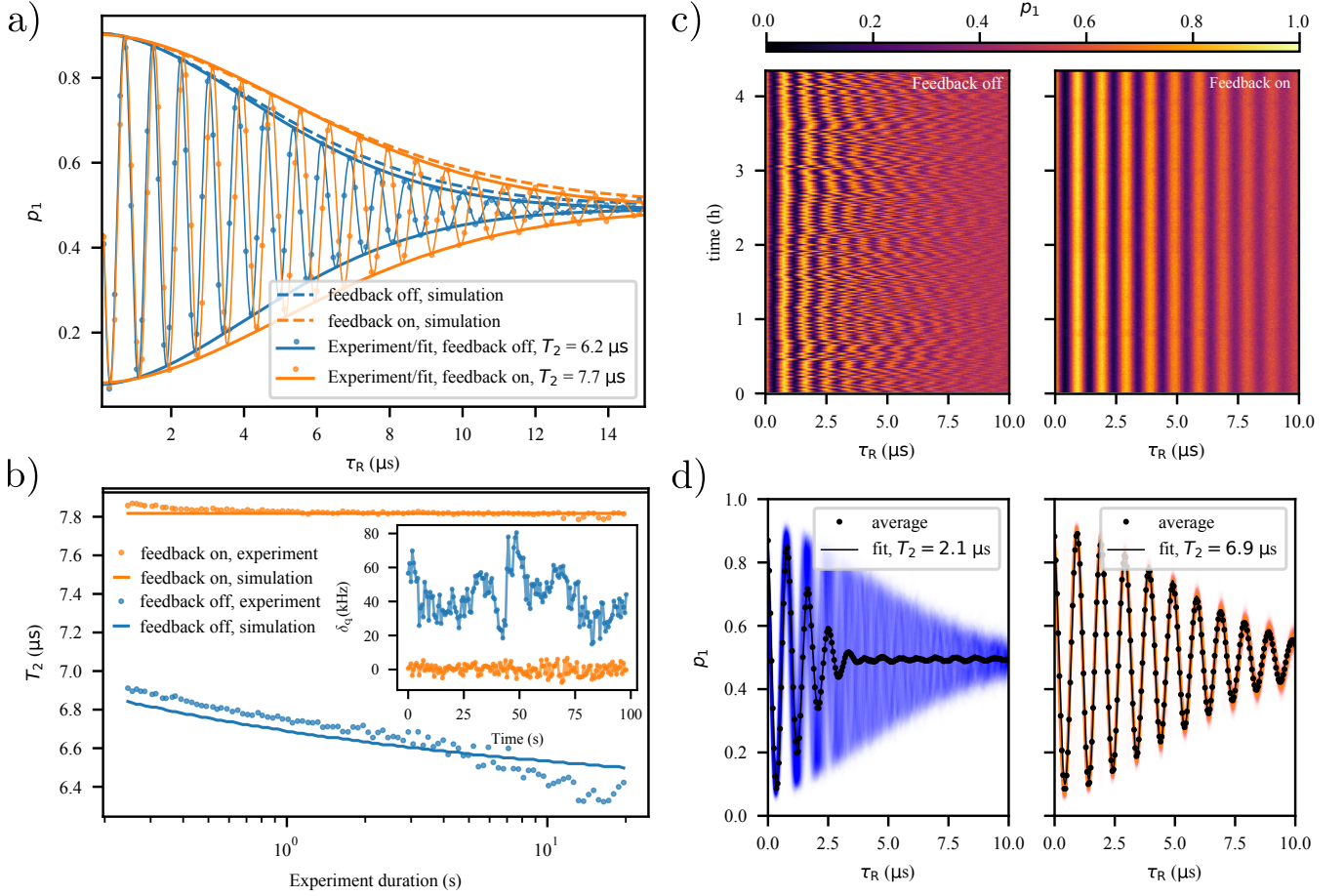


FIG. 2. Improvement in qubit coherence and stability a) The coherence time T_2 of the qubit is measured by interleaving a Ramsey measurement with feedback sequences (orange dots), compared to when the feedback is off (blue dots). The solid lines are a fit to the data. Dashed lines show a simulation of the decay envelope assuming the noise spectral densities shown in Fig. 1d. b) The measured coherence time of the qubit as a function of the duration of the Ramsey experiment is shown with the feedback (orange dots) and without (blue dots). The solid lines are the expected coherence times based on the measured noise spectral density. The inset shows the measured deviation of the qubit frequency from the target frequency during the experiment. Each point is calculated using 50 averages of the Ramsey trace. Panel c) shows Ramsey experiment repeated for 4 hours with (right) and without (left) feedback. With the feedback, the qubit frequency is stable during the whole duration. d) Averaging the data in panel c) results in significant reduction in qubit coherence if feedback is not used (left). Using the feedback, the inferred coherence is not affected by the measurement duration (right). The coherence time of a single Ramsey trace here is slightly lower than in a) due to smaller value of $\tau = 500 \text{ ns}$ used in the feedback.

frequency estimation without the feedback is shown with solid blue line in Fig. 1d, matching the experiment almost perfectly. The solid orange line shows the simulated qubit frequency estimates when the feedback is turned on, again matching well with the experiment. Finally, using the simulation we can calculate the power spectral density of the real qubit frequency fluctuations when the feedback is applied, shown with solid red line in Fig. 1d. The total noise power mitigated by the feedback protocol is indicated by the shaded area in Fig. 1d.

B. Qubit coherence

Next, we interleave the frequency estimation sequences with a Ramsey experiment to demonstrate that the lower noise power increases the qubit coherence time T_2 , see schematic in Fig. 1b. We apply two $\pi/2$ pulses around the y -axis of the Bloch sphere, and sweep the delay between the pulses, τ_R . Fig. 2a shows the qubit excited state population p_1 going through the Ramsey oscillations, first without the feedback, and then with the feedback turned on. For a Gaussian-distributed noise process, the envelope of the Ramsey oscillations decays

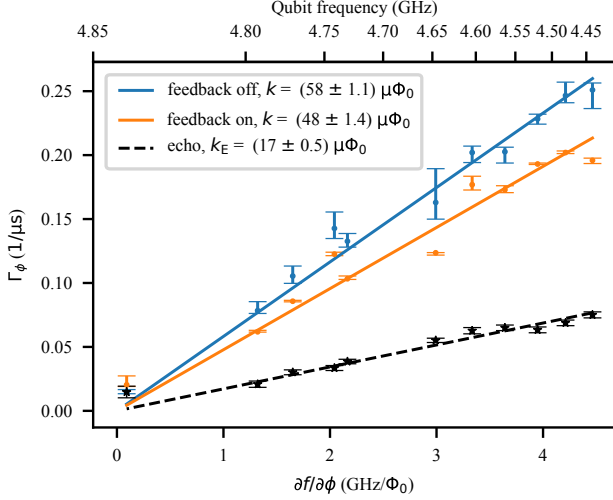


FIG. 3. **Qubit coherence at different bias points** a) The qubit dephasing rate Γ_ϕ is evaluated at several different bias fluxes. Qubit's sensitivity to flux noise increases further away from the sweet spot, resulting in reduced dephasing times (increased dephasing rates). The error bars show 68% confidence intervals for the median of the dephasing times measured 60 times. The solid lines show a linear fit to the dephasing rates with respect to the curvature of the qubit spectrum with respect to flux. The black stars show the dephasing times extracted from a spin-echo experiment, used as a reference.

as [27]

$$\chi_R(t) = \exp \left[-2t^2 \pi^2 \int_{f_0}^{\infty} S_{f_q f_q}(f) \text{sinc}^2(\pi f t) df \right], \quad (5)$$

where $S_{f_q f_q}(f)$ is the unilateral power spectral density of the frequency fluctuations and f_0 is the lower cutoff frequency equal to the inverse of the total duration of the experiment. We fit the experimental data to an oscillating function with a decay envelope corresponding to a power spectral density of $1/f$ noise and extract the coherence time from when the decay envelope drops below $1/e$ from its original value at $t_R = 0$. The feedback increases the coherence time from $T_2 = 6.2 \mu\text{s}$ to $T_2 = 7.7 \mu\text{s}$, or 26%. The observed improvement in coherence time was consistent across several repetitions of the experiment. The fitted decay envelope can be compared to a theoretical estimate obtained by directly substituting the measured power spectra to Eq. (5), shown with dashed lines in Fig. 2a, closely matching experimentally observed decay envelopes. The only fit parameter is the qubit state initialization fidelity, 92%, which scales the decay envelope amplitude. This confirms that the decoherence of the qubit is well described by the measured power spectral density of the frequency fluctuations.

The inferred coherence time of the qubit depends on the total duration of the Ramsey experiment through the cutoff frequency f_0 in Eq. (5). In Fig. 2b, the coherence time T_2 is evaluated using different numbers of averages

to calculate p_1 , thereby changing the total duration of the single Ramsey experiment and the cutoff frequency f_0 . The data from the experiment is collected only once, and is sectioned to different numbers of averages as post-processing. Without the feedback, the coherence time gradually decreases as the duration of the experiment increases. This is due to the increased noise power at lower frequencies for $1/f$ noise. When the feedback is activated, the overall coherence time is increased — similar to the experiment shown in Fig. 2a — and remains constant independent of the cutoff frequency f_0 due to the elimination of the low frequency noise. Moreover, the qubit frequency remains stable during the measurement, as inferred from the frequency of the Ramsey oscillations during the experiment, shown in inset of Fig. 2b. The qubit frequencies in the inset are evaluated from a running average of 50 Ramsey traces.

The stability of the qubit frequency can be maintained for hours using the feedback protocol as demonstrated in Fig. 2c. There, Ramsey experiments are repeated for more than four hours, either with the feedback turned off (left panel) or on (right panel). When the measured qubit excited state populations are overlaid (Fig. 2d), the Ramsey oscillations without the feedback are blurred due to the constant fluctuation in the qubit frequency, whereas with the feedback the oscillations are clearly visible. The coherence time extracted from the average of all uncorrected (feedback off) Ramsey experiments is only $T_2 = 2.1 \mu\text{s}$, compared to $T_2 = 6.9 \mu\text{s}$ with the feedback.

Thus far, we have operated the qubit at a fixed flux bias point. We next demonstrate that the feedback protocol improves the coherence time for a range of flux biases. The sensitivity of the qubit to the flux noise is determined by the curvature of its frequency spectrum with respect to flux bias, allowing us to probe the efficiency of the feedback at various noise levels and intrinsic coherence times. We evaluate the pure dephasing rate of the qubit at 11 different bias points, first without the feedback and then with it on. The pure dephasing rates are extracted from the decay of the Ramsey oscillations by subtracting the effect of the energy-relaxation rate [9]. The measured dephasing rates (Fig. 3) are lowest close to the flux sweet spot and gradually increase away from this spot as the qubit sensitivity to the noise increases. In the limit where decoherence is dominated by flux noise, Eq. (5) can be used to show that there is an (almost) linear dependence between the dephasing rate Γ_ϕ and the flux sensitivity of the qubit [9, 27],

$$\Gamma_\phi = k \left| \frac{\partial f_q}{\partial \Phi} \right|. \quad (6)$$

We find the coefficient k from a linear fit to the data in Fig. 3a and use the result to assess the impact of the feedback on mitigating the flux noise. Without the feedback $k = (58 \pm 1.1) \mu\Phi_0$, and reduces to $k = (48 \pm 1.4) \mu\Phi_0$ when the feedback is used, an improvement of 17%. This implies that the feedback effectively reduces the flux noise amplitude seen by the qubit.

The ultimate goal would be to suppress the low frequency noise to the level that the coherence time measured using a spin echo experiment — which is insensitive to low frequency noise — would be equal or higher than the coherence time in a feedback stabilized Ramsey experiment. In Fig. 3a, the dephasing rate measured from an echo experiment are shown with black dots, and the linear fit yields $k_E = (17 \pm 0.5) \mu\Phi_0$, which corresponds to the $1/f$ flux-noise amplitude of $\sqrt{A_\Phi} = (3.3 \pm 0.1) \mu\Phi_0$, see Supplementary material for additional information. The main reason why the impact of the noise on the echo experiment is lower than the on feedback-stabilized Ramsey experiment is the limited bandwidth of our feedback implementation. While the feedback efficiently suppresses the noise up to 1 kHz, the echo experiment is mostly insensitive to the noise below the inverse duration of a single echo experiment, here approximately ~ 100 kHz.

Unlike the spin echo experiment, which is specifically designed to be insensitive to the low frequency qubit frequency fluctuations, many quantum algorithms or sequences of quantum gates are highly sensitive to small deviations in the qubit frequency. While there exist several open-loop control strategies for minimizing gate sensitivity to noise at different frequencies [28, 29], there is always an added cost in the duration of the gate sequence or complexity in calibration. The advantage of the feedback based stabilization method is that no changes to the gate sequences or controls are required.

C. Randomized benchmarking

Next, we demonstrate that the feedback protocol improves the single-qubit gate fidelity in our device. We bias the qubit 400 MHz away from the flux sweet spot so that it is highly sensitive to flux noise and perform single-qubit randomized benchmarking [31] while stabilizing the qubit frequency with the feedback. Fig. 4a shows the qubit excited state population p_1 as a function of number of Clifford gates in a random sequence, followed by a Clifford gate that would ideally bring the qubit back to the ground state. With the feedback off (blue) and on (orange), the experiment is repeated for 50 different random sequences, which are averaged and used to find the average error per gate [30]. The feedback reduces the average error per gate from $(8.5 \pm 2.1) \times 10^{-4}$ to $(5.9 \pm 0.7) \times 10^{-4}$, approaching the limit imposed by the energy-relaxation rate of the qubit, see Supplementary material for additional information. While such fidelities are commonly observed at or near the flux-insensitive point in many devices [30, 32], it is unusual to see it so far from the sweet spot.

We attribute the reduction in the average gate error mostly to the improved stability of the qubit frequency. Without feedback, several of the random sequences show oscillating decay functions with the number of Clifford gates, indicative of coherent control errors, such as the

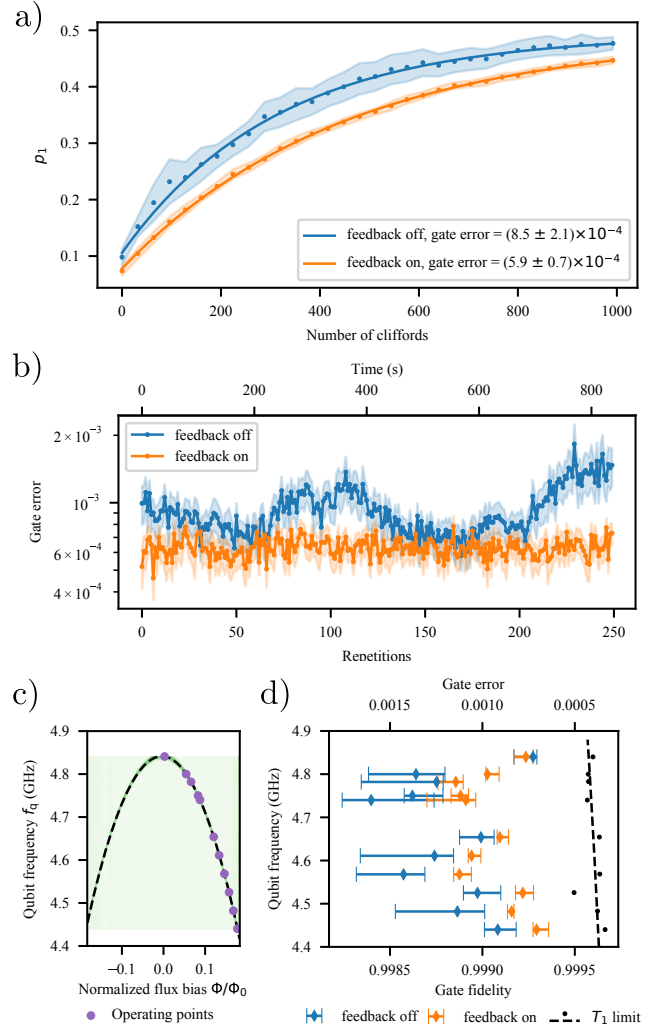


FIG. 4. **Randomized benchmarking** a) Randomized benchmarking of the single qubit gates at $f_q = 4.44$ GHz. The orange (blue) dots show the average of 50 realizations of the random Clifford sequences with (without) the feedback. The shaded area shows the 68% confidence interval for the average trajectory. The gate error is extracted from the fit to the data (solid line). b) Randomized benchmarking is repeated 250 times with the feedback (orange dots) and then without (blue dots). The shaded area shows the 68% confidence interval of the fitted gate error. c) The qubit spectrum and the operating points at which the gate errors are evaluated in d). d) Randomized benchmarking at several different qubit bias fluxes. Black dots show the estimated coherence limit for the gate fidelities, inferred from the energy relaxation time T_1 of the qubit [30]. The dashed black line shows a linear fit to the estimated coherence limits at the different operating points.

quasi-static shifts in the qubit frequency due to the low frequency noise. In contrast, with the feedback activated, the function monotonically decays for all random sequences, something that is typical for incoherent errors [33, 34]. This observation is supported by the experiment in Fig. 4b where we show the gate errors inferred from randomized benchmarking experiments re-

peated 250 times with 7 different realizations of a random gate sequence, for a total duration of 840 s. Without the feedback, we observe a significant drift in the gate errors. With feedback turned on, the gate errors remain consistently low, indicating that the feedback successfully stabilized the drift and fluctuations in the qubit frequency. This is also manifested in lowered uncertainty in the fitted gate error in Fig. 4a.

We observe a similar improvement on gate fidelity for all flux bias points with the exception of the sweet spot, see Figs. 4c and d. At each flux point, we repeated the randomized benchmarking experiment 10 times with and without feedback, re-calibrating the qubit frequency between every repetition of the randomized benchmarking experiment. In contrast to the coherence time T_2 — which is the highest at the sweet spot and then consistently decreases as the flux noise sensitivity increases away from the sweet spot — the highest gate fidelities are in fact measured at the most flux-sensitive point we investigated. We attribute the increasing trend in the fidelities at lower frequencies to the higher energy-relaxation time T_1 of the qubit. Additionally, spectrally moving parasitic two-level fluctuators reduced the best achievable single-qubit gate fidelities at certain bias points. Due to the coupling to the qubit, the changes in the frequencies of the two-level fluctuators caused shifts in the qubit frequency. As a result, at some bias points there were wide variations in the measured gate fidelities between different experiments, which are responsible for the large error bars in Fig. 4c when the feedback was not used. The variation is significantly reduced by the feedback, as indicated by the repetition experiment shown in Fig. 4b and further verified in Fig. 4c. This highlights that the implemented feedback protocol can mitigate the impact of many sources of low-frequency noise, such as frequency shifts caused by two-level fluctuators.

III. CONCLUSIONS

In this work we have implemented a closed-loop feedback protocol to stabilize the drift and fluctuations in the frequency of a superconducting transmon qubit. In the probing phase we use repeated Ramsey experiments to estimate the qubit frequency and adjust the qubit frequency to cancel the measured frequency offset. The probing phase can be interleaved with a computational workload such as algorithm execution.

We have demonstrated that the feedback stabilizes the qubit frequency fluctuations even when the qubit is not operated at the noise-insensitive operation point. This leads to reduction in the noise power observed by the qubit, resulting in improved coherence times and improved gate fidelities. The ability to operate qubits away from the protected bias point will help addressing the frequency crowding problem in large quantum processors by increasing the operable frequency band for the qubits. Additionally, the increased operable frequency band helps to avoid spurious modes arising for example from two-level fluctuators.

While in this work we have mostly focused on mitigating $1/f$ -flux noise, the feedback algorithm is agnostic to the source of the noise in the qubit frequency. The proposed technique should work equally well on other low-frequency noise sources, such as charge noise or TLS induced shifts in the qubit frequency. Moreover, the feedback relies only on single-qubit operations which implies that it can be extended to multi-qubit systems without additional cost in time or complexity.

ACKNOWLEDGMENTS

This work was supported in part by the U.S. Army Research Office (ARO) Grant W911NF-18-1-0411; by the ARO Multi-University Research Initiative W911NF-18-1-0218; and by the Assistant Secretary of Defense for Research and Engineering via MIT Lincoln Laboratory under Air Force Contract No. FA8721-05-C-0002. A.K. acknowledges support from the NSF Graduate Research Fellowship program.

-
- [1] D. A. Steck, K. Jacobs, H. Mabuchi, T. Bhattacharya, and S. Habib, Quantum feedback control of atomic motion in an optical cavity, *Phys. Rev. Lett.* **92**, 223004 (2004).
 - [2] D. J. Wilson, V. Sudhir, N. Piro, R. Schilling, A. Ghadimi, and T. J. Kippenberg, Measurement-based control of a mechanical oscillator at its thermal decoherence rate, *Nature* **524**, 325 (2015).
 - [3] R. Vijay, C. Macklin, D. Slichter, S. Weber, K. Murch, R. Naik, A. N. Korotkov, and I. Siddiqi, Stabilizing rabi oscillations in a superconducting qubit using quantum feedback, *Nature* **490**, 77 (2012).
 - [4] M. D. Shulman, S. P. Harvey, J. M. Nichol, S. D. Bartlett, A. C. Doherty, V. Umansky, and A. Yacoby, Suppressing qubit dephasing using real-time hamiltonian estimation, *Nature communications* **5**, 1 (2014).
 - [5] T. Nakajima, A. Noiri, K. Kawasaki, J. Yoneda, P. Stano, S. Amaha, T. Otsuka, K. Takeda, M. R. Delbecq, G. Allison, A. Ludwig, A. D. Wieck, D. Loss, and S. Tarucha, Coherence of a driven electron spin qubit actively decoupled from quasi-static noise, *Phys. Rev. X* (2020).
 - [6] S. Majumder, L. A. de Castro, and K. R. Brown, Real-time calibration with spectator qubits, *npj Quantum Information* **6**, 1 (2020).

- [7] F. Yan, S. Gustavsson, A. Kamal, J. Birenbaum, A. P. Sears, D. Hover, T. J. Gudmundsen, D. Rosenberg, G. Samach, S. Weber, *et al.*, The flux qubit revisited to enhance coherence and reproducibility, *Nature communications* **7**, 1 (2016).
- [8] G. Catelani, R. J. Schoelkopf, M. H. Devoret, and L. I. Glazman, Relaxation and frequency shifts induced by quasiparticles in superconducting qubits, *Physical Review B* **84**, 064517 (2011).
- [9] J. Bylander, S. Gustavsson, F. Yan, F. Yoshihara, K. Harrabi, G. Fitch, D. G. Cory, Y. Nakamura, J.-S. Tsai, and W. D. Oliver, Noise spectroscopy through dynamical decoupling with a superconducting flux qubit, *Nature Physics* **7**, 565 (2011).
- [10] J. Braumüller, L. Ding, A. P. Vepsäläinen, Y. Sung, M. Kjaergaard, T. Menke, R. Winik, D. Kim, B. M. Niedzielski, A. Melville, *et al.*, Characterizing and optimizing qubit coherence based on squid geometry, *Physical Review Applied* **13**, 054079 (2020).
- [11] M. McEwen, L. Faoro, K. Arya, A. Dunsworth, T. Huang, S. Kim, B. Burkett, A. Fowler, F. Arute, J. C. Bardin, *et al.*, Resolving catastrophic error bursts from cosmic rays in large arrays of superconducting qubits, *arXiv preprint arXiv:2104.05219* (2021).
- [12] C. Wilen, S. Abdullah, N. Kurinsky, C. Stanford, L. Cardani, G. d'Imperio, C. Tomei, L. Faoro, L. Ioffe, C. Liu, *et al.*, Correlated charge noise and relaxation errors in superconducting qubits, *arXiv preprint arXiv:2012.06029* (2020).
- [13] A. P. Vepsäläinen, A. H. Karamlou, J. L. Orrell, A. S. Dogra, B. Loer, F. Vasconcelos, D. K. Kim, A. J. Melville, B. M. Niedzielski, J. L. Yoder, *et al.*, Impact of ionizing radiation on superconducting qubit coherence, *Nature* **584**, 551 (2020).
- [14] J. Koch, M. Y. Terri, J. Gambetta, A. A. Houck, D. Schuster, J. Majer, A. Blais, M. H. Devoret, S. M. Girvin, and R. J. Schoelkopf, Charge-insensitive qubit design derived from the cooper pair box, *Physical Review A* **76**, 042319 (2007).
- [15] M. Kjaergaard, M. E. Schwartz, J. Braumüller, P. Krantz, J. I.-J. Wang, S. Gustavsson, and W. D. Oliver, Superconducting qubits: Current state of play, *Annual Review of Condensed Matter Physics* **11**, 369 (2020).
- [16] F. Arute, K. Arya, R. Babbush, D. Bacon, J. C. Bardin, R. Barends, R. Biswas, S. Boixo, F. G. Brandao, D. A. Buell, *et al.*, Quantum supremacy using a programmable superconducting processor, *Nature* **574**, 505 (2019).
- [17] R. Barends, J. Kelly, A. Megrant, A. Veitia, D. Sank, E. Jeffrey, T. C. White, J. Mutus, A. G. Fowler, B. Campbell, *et al.*, Superconducting quantum circuits at the surface code threshold for fault tolerance, *Nature* **508**, 500 (2014).
- [18] P. Krantz, M. Kjaergaard, F. Yan, T. P. Orlando, S. Gustavsson, and W. D. Oliver, A quantum engineer's guide to superconducting qubits, *Applied Physics Reviews* **6**, 021318 (2019).
- [19] P. Klimov, J. Kelly, Z. Chen, M. Neeley, A. Megrant, B. Burkett, R. Barends, K. Arya, B. Chiaro, Y. Chen, *et al.*, Fluctuations of energy-relaxation times in superconducting qubits, *Physical review letters* **121**, 090502 (2018).
- [20] S. de Graaf, L. Faoro, L. Ioffe, S. Mahashabde, J. Burnett, T. Lindström, S. Kubatkin, A. Danilov, and A. Y. Tzalenchuk, Two-level systems in superconducting quantum devices due to trapped quasiparticles, *arXiv preprint arXiv:2004.02485* (2020).
- [21] J. J. Burnett, A. Bengtsson, M. Scigliuzzo, D. Niepce, M. Kudra, P. Delsing, and J. Bylander, Decoherence benchmarking of superconducting qubits, *npj Quantum Information* **5**, 1 (2019).
- [22] S. Schlör, J. Lisenfeld, C. Müller, A. Bilmes, A. Schneider, D. P. Pappas, A. V. Ustinov, and M. Weides, Correlating decoherence in transmon qubits: Low frequency noise by single fluctuators, *Physical review letters* **123**, 190502 (2019).
- [23] A. Wallraff, D. Schuster, A. Blais, L. Frunzio, J. Majer, M. Devoret, S. Girvin, and R. Schoelkopf, Approaching unit visibility for control of a superconducting qubit with dispersive readout, *Physical review letters* **95**, 060501 (2005).
- [24] M. Rol, C. Bultink, T. O'Brien, S. De Jong, L. Theis, X. Fu, F. Luthi, R. Vermeulen, J. de Sterke, A. Bruno, *et al.*, Restless tuneup of high-fidelity qubit gates, *Physical Review Applied* **7**, 041001 (2017).
- [25] M. Werninghaus, D. Egger, and S. Filipp, High-speed calibration and characterization of superconducting quantum processors without qubit reset, *arXiv preprint arXiv:2010.06576* (2020).
- [26] F. Yan, J. Bylander, S. Gustavsson, F. Yoshihara, K. Harrabi, D. G. Cory, T. P. Orlando, Y. Nakamura, J.-S. Tsai, and W. D. Oliver, Spectroscopy of low-frequency noise and its temperature dependence in a superconducting qubit, *Physical Review B* **85**, 174521 (2012).
- [27] G. Ithier, E. Collin, P. Joyez, P. Meeson, D. Vion, D. Esteve, F. Chiarello, A. Shnirman, Y. Makhlin, J. Schrieffer, *et al.*, Decoherence in a superconducting quantum bit circuit, *Physical Review B* **72**, 134519 (2005).
- [28] S. Sheldon, E. Magesan, J. M. Chow, and J. M. Gambetta, Procedure for systematically tuning up crosstalk in the cross-resonance gate, *Physical Review A* **93**, 060302 (2016).
- [29] A. R. Milne, C. L. Edmunds, C. Hempel, F. Roy, S. Mavadia, and M. J. Biercuk, Phase-modulated entangling gates robust to static and time-varying errors, *Physical Review Applied* **13**, 024022 (2020).
- [30] Z. Chen, *Metrology of quantum control and measurement in superconducting qubits*, Ph.D. thesis, UC Santa Barbara (2018).
- [31] E. Knill, D. Leibfried, R. Reichle, J. Britton, R. B. Blakestad, J. D. Jost, C. Langer, R. Ozeri, S. Seidelin, and D. J. Wineland, Randomized benchmarking of quantum gates, *Physical Review A* **77**, 012307 (2008).
- [32] Y. Sung, L. Ding, J. Braumüller, A. Vepsäläinen, B. Kannan, M. Kjaergaard, A. Greene, G. O. Samach, C. McNally, D. Kim, *et al.*, Realization of high-fidelity cz and zz-free iswap gates with a tunable coupler, *arXiv preprint arXiv:2011.01261* (2020).
- [33] Y. R. Sanders, J. J. Wallman, and B. C. Sanders, Bounding quantum gate error rate based on reported average fidelity, *New Journal of Physics* **18**, 012002 (2015).
- [34] A. Greene, M. Kjaergaard, M. Schwartz, G. Samach, A. Bengtsson, M. O'Keeffe, D. Kim, M. Marvian, A. Melville, B. Niedzielski, *et al.*, Error mitigation via stabilizer measurement emulation, *arXiv preprint arXiv:2102.05767* (2021).
- [35] S. Danilin, A. V. Lebedev, A. Vepsäläinen, G. B. Lesovik, G. Blatter, and G. Paraoanu, Quantum-enhanced mag-

- netometry by phase estimation algorithms with a single artificial atom, npj Quantum Information **4**, 1 (2018).
- [36] A. Oppenheim, R. Schafer, and J. Buck, *Discrete-time Signal Processing*, Prentice Hall International Editions Series (Prentice Hall, 1999).
 - [37] P. O'Malley, J. Kelly, R. Barends, B. Campbell, Y. Chen, Z. Chen, B. Chiaro, A. Dunsworth, A. Fowler, I.-C. Hoi, *et al.*, Qubit metrology of ultralow phase noise using randomized benchmarking, Physical Review Applied **3**, 044009 (2015).

SUPPLEMENTARY MATERIAL: IMPROVING QUBIT COHERENCE USING CLOSED-LOOP FEEDBACK

A. Qubit frequency estimation

The qubit frequency can be estimated using a simple version of the single qubit phase estimation algorithm where the qubit is first prepared in a superposition state with a $\pi/2$ rotation around Y axis followed by free evolution. During the free evolution, the qubit wavefunction accumulates a phase (in the frame rotating with the drive) $\phi(t) = \int_0^t 2\pi\delta_q(t)dt$, where $\delta_q(t) = f_d - f_q(t)$ and f_d and $f_q(t)$ are the drive frequency and the qubit frequency. The accumulated phase can be estimated by measuring either $\langle X \rangle$ or $\langle Y \rangle$. During the experiment, the qubit state evolves as

$$|\psi\rangle = \exp\left(-\frac{i\pi}{4}M\right) \exp\left(-i\frac{\pi}{2}\phi(\tau)Z\right) \exp\left(-\frac{i\pi}{4}Y\right)|\psi_0\rangle, \quad (\text{S1})$$

where $|\psi_0\rangle$ is the initial state of the qubit, τ is the free-evolution time, M is the measurement operator, and $\phi(\tau) = 2\pi\tau\delta_q$ if the detuning δ_q is assumed to be constant during the experiment. The probability of measuring the excited state is given by

$$p_1 = \frac{1 - \langle\psi|Z|\psi\rangle}{2} = \frac{1}{2} + \frac{1}{2}\cos(2\pi\delta_q\tau - \phi_m), \quad (\text{S2})$$

where ϕ_m is a phase factor that depends on the measurement operator,

$$\phi_m = \begin{cases} 0, & \text{if } M = X, \\ \pi/2, & \text{if } M = Y. \end{cases} \quad (\text{S3})$$

Solving for δ_q yields

$$\delta_q = \frac{\pm \arccos(2p_1 - 1) + \phi_m + 2\pi k}{2\pi\tau}. \quad (\text{S4})$$

By choosing $k = 0$ and the negative branch δ_q is uniquely defined in the range $\delta_q = [\frac{\phi_m - \pi}{2\pi\tau}, \frac{\phi_m}{2\pi\tau}]$, which is symmetric around zero for $\phi_m = \frac{\pi}{2}$.

The qubit excited state probability \hat{p}_1 can be estimated from N measurements of the qubit state q_i through $\hat{p}_1 = \frac{1}{N} \sum_{i=0}^N q_i$, which then gives an estimate of the qubit frequency $\hat{\delta}_q$. However, this frequency estimate is noisy due to finite number of samples used to estimate the excited state probability. The impact of the noise can be estimated by noting that \hat{p}_1 is binomially distributed, and its standard deviation is

$$\delta\hat{p}_1 = \sqrt{\frac{p_1(1-p_1)}{N}} = \frac{1}{2\sqrt{N}}, \text{ for } p = 1/2. \quad (\text{S5})$$

The error in the frequency estimate is then given by

$$\delta\hat{\delta}_q = \left| \frac{\partial\delta_q}{\partial p_1} \delta\hat{p}_1 \right| \approx \left| \frac{\partial}{\partial p_1} \frac{\frac{\pi}{2} + \phi_m + 2p_1 - 1}{2\pi\tau} \delta\hat{p}_1 \right| = \frac{1}{2\pi\tau\sqrt{N}}, \quad (\text{S6})$$

where δ_q has been expanded to the first order in p_1 . This implies that the estimation noise can be reduced either by increasing τ or the number of measurements used in the estimation. However, the bandwidth of the estimation algorithm is limited by the requirement that each frequency has to be uniquely given by p_1 . This is true if $|\delta_q\tau| \leq \frac{1}{4}$. As a result, there is a trade-off between the estimation bandwidth and sensitivity. Decoherence further reduces the sensitivity, and the optimum is obtained at $\tau = T_2$ [35]. In practice, τ often needs to be shorter to satisfy the bandwidth requirement. Using a larger N increases the total time taken by the frequency estimation, which reduces the repetition rate of the feedback algorithm.

B. Circuit analysis

Here we theoretically analyze the implemented feedback circuit and assess its performance. We start by writing the block diagram for the circuit, shown in S1a. In the diagram and the following calculation, the quantities are sampled

at times $t = nT_N = nNT$, where T is the total duration of a Ramsey experiment and N is the number of Ramsey experiments used to estimate the qubit frequency. The target qubit frequency is controlled by $d[n] = f_d$ which we keep fixed at all times. At every cycle of the feedback, the target frequency $d[n]$ is compared to the estimated qubit frequency $f[n]$, resulting in the error signal $e[n] = d[n] - (f[n] + v[n])$, where $v[n]$ is the sampling noise. In the experiment, the error signal is given by $e[n] = \hat{\delta}_q[n]$, and the sampling noise $v[n] = \delta\hat{\delta}_q[n]$ is defined in Eq. (S6). The error signal is multiplied by a controllable gain G , and is fed to an accumulator outputting the feedback control signal $p[n-1]$ — delayed by one time step — which then adjusts the qubit frequency.

The sampled qubit frequency $f[n]$ is estimated from the real qubit frequency $f_q(t)$ using N Ramsey measurements as described in the main text. Here, we approximate the sampled frequency as the average qubit frequency during the sampling

$$f[n] \approx \frac{1}{N\tau} \sum_{i=0}^{N-1} \int_{nT_N+iT}^{nT_N+iT+\tau} f_q(t) dt. \quad (\text{S7})$$

The qubit frequency is determined by its intrinsic fluctuating value \tilde{f}_q which is acted on by the feedback signal $p[n-1]$ so that $f_q(t) = \tilde{f}_q(t) + p[n-1]$. Substituting to Eq. (S7) yields

$$f[n] \approx p[n-1] + \frac{1}{N\tau} \sum_{i=0}^{N-1} \int_{nT_N+iT}^{nT_N+iT+\tau} \tilde{f}_q(t) dt \equiv p[n-1] + \tilde{f}[n], \quad (\text{S8})$$

forming the feedback loop.

To analyze the impact of the feedback on the signal and the sampling noise, we start by solving the transfer function of the feedback signal $p[n]$ from

$$\begin{aligned} e[n] &= d[n] - v[n] - \tilde{f}[n] - p[n-1], \\ p[n] &= p[n-1] + y[n], \\ y[n] &= Ge[n], \\ \implies p[n] &= p[n-1] - G(-d[n] + v[n] + \tilde{f}[n] + p[n-1]). \end{aligned} \quad (\text{S9})$$

Applying the z -transform yields

$$\begin{aligned} P(z) &= z^{-1}P(z) - G(-D(z) + V(z) + \tilde{F}(z) + z^{-1}P(z)), \\ P(z) &= \frac{G(D(z) - V(z) - \tilde{F}(z))}{1 - z^{-1} + z^{-1}G}, \end{aligned} \quad (\text{S10})$$

resulting in the transfer function

$$X_p(z) = P(z)/(D(z) - V(z) - \tilde{F}(z)) = \frac{G}{1 - z^{-1} + z^{-1}G}. \quad (\text{S11})$$

To get the frequency response $H_p(f)$ from the transfer function in Eq. (S11), we substitute $z = e^{i2\pi fNT}$ so that $H_p(f) = X_p(e^{i2\pi fNT})$, which is shown in Fig. S1b for $G = 0.35$. The power spectral density of the feedback signal as a response to the frequency fluctuations of the system is given by the squared magnitude of the frequency response [36]

$$S_{pp}(f) = |H_p(f)|^2 S_{ss}(f), \quad (\text{S12})$$

where $S_{ss}(f)$ is the combined power spectral density of the target signal $d[n]$, the sampled intrinsic qubit frequency $\tilde{f}[n]$ and the sampling noise $v[n]$, $S_{ss}(f) = S_{dd}(f) + S_{ff}(f) + S_{vv}(f)$. We assume that there is only a minimal amount of noise in frequency of the microwave source which sets the target frequency, implying that we can set $S_{dd} \approx 0$. To maximize the efficiency of the feedback, we limit the bandwidth of the frequency response to the frequencies where the spectral density of the qubit frequency fluctuations is higher than the sampling noise. Another option would be to increase number of phase sampling experiments N per frequency estimate, which reduces the sampling noise power at the cost of a longer total time used for feedback.

To better understand the experimentally measured spectrum in Fig. 1d of the main text, we next calculate the

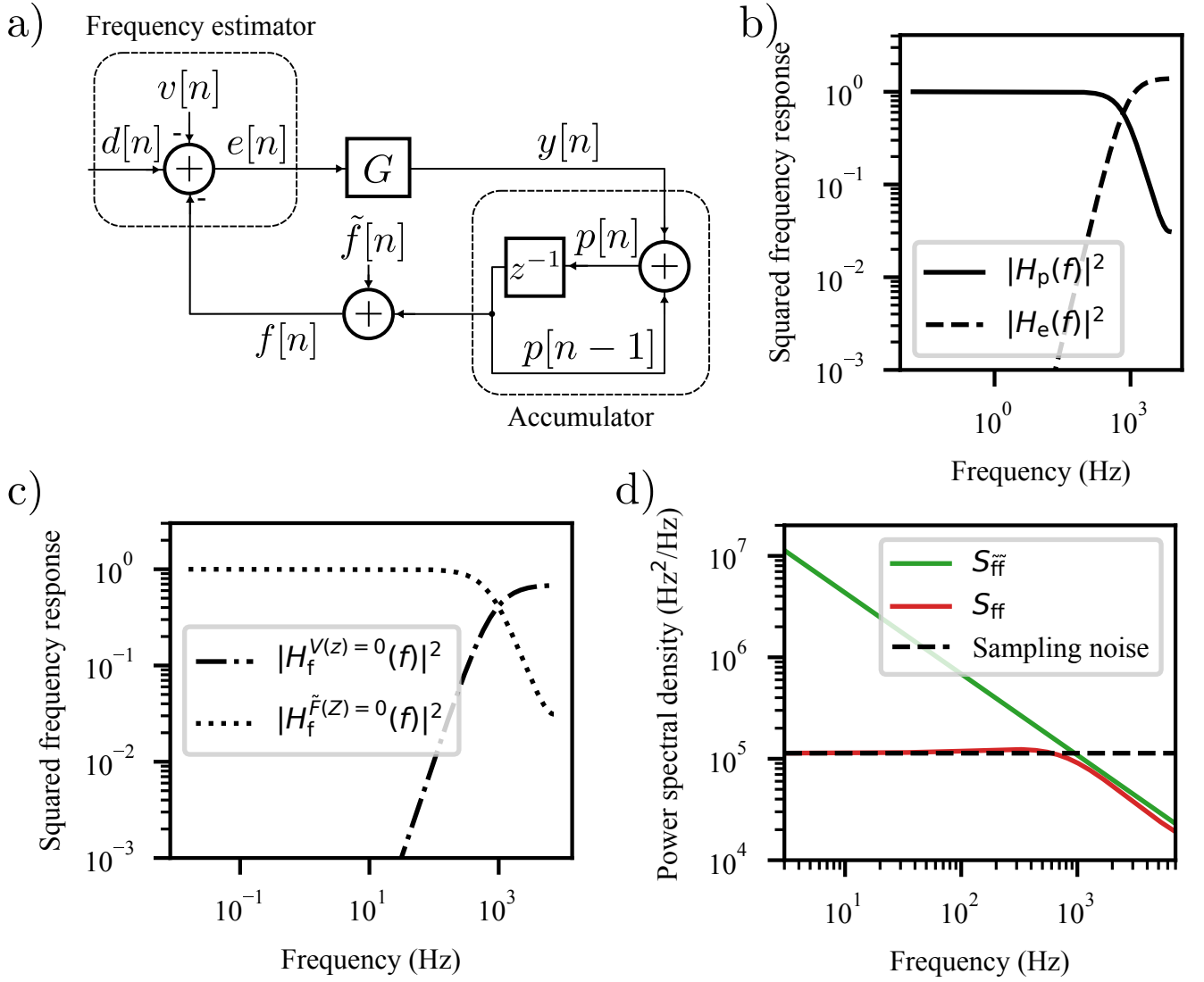


FIG. S1. a) The diagram of the feedback circuit. b) The squared magnitude of the frequency responses for the control and error signals $p[n]$ and $e[n]$. c) The squared magnitude of the frequency response for the qubit frequency during the feedback. The dashed line shows the frequency response of the qubit to the sampling noise, and the dash-dotted line shows the frequency response to the fluctuations in the intrinsic qubit frequency. d) The power spectral density of the qubit frequency fluctuation with the feedback activated (red) calculated using the frequency responses shown in c) and the experimentally measured spectral density of the intrinsic qubit frequency fluctuation (green). The dashed line shows the sampling noise.

frequency response of the error signal $e[n]$ from Eqs. (S9). Applying the z -transform and solving for $E(z)$ yields

$$\begin{aligned}
 E(z) &= D(z) - V(z) - \tilde{F}(z) - z^{-1}P(z), \\
 P(z) &= z^{-1}P(z) + GE(z), \\
 \Rightarrow E(z) &= \frac{1 - z^{-1}}{1 - z^{-1} + Gz^{-1}}(D(z) - V(z) - \tilde{F}(z)), \\
 \Rightarrow X_e(z) &= \frac{1 - z^{-1}}{1 - z^{-1} + Gz^{-1}}.
 \end{aligned} \tag{S13}$$

The frequency response $H_e(f) = X_e(e^{i2\pi fNT})$ is plotted in Fig. S1b. Without the feedback, the expected spectral density of the error signal is $S_{ee}^{\text{nofeedback}}(f) = S_{ff}(f) + S_{vv}(f)$. When the feedback is turned on, the response is $S_{ee}^{\text{feedback}} = (S_{ff}(f) + S_{vv}(f))|H_e(f)|^2$ instead. At lower frequencies, the frequency response of the error signal goes

down, explaining the observed behavior in the spectra in Fig. 1b in the main text. Because the sampling noise in the frequency estimation affects the qubit frequency through the feedback, the spectral density of the error signal does not exactly match the spectral density of the real qubit frequency.

We now analyze the impact of the feedback directly on the noise spectral density of the qubit frequency. We first calculate the transfer function $X_f(z) = \frac{F(z)}{D(z) - V(z) - \tilde{F}(z)}$ of the qubit frequency $f[n]$ right after a feedback cycle when $f[n] = p[n] + \tilde{f}[n]$. Using the result of Eq. (S10) we get

$$\begin{aligned} X_f(z) &= \frac{\tilde{F}(z)}{D(z) - V(z) - \tilde{F}(z)} + X_p(z) \\ \implies X_f(z) &= \begin{cases} X_p(z) - 1, & \text{for } V(z) = 0 \text{ and } D(z) = 0 \\ X_p(z), & \text{for } \tilde{F}(z) = 0 \text{ and } D(z) = 0. \end{cases} \end{aligned} \quad (\text{S14})$$

The squared magnitude of the frequency responses of these transfer functions, $|H_f^{F(\tilde{z})=0}(f)|^2$ and $|H_f^{V(\tilde{z})=0}(f)|^2$, are plotted in Fig. S1c. The spectral density of the qubit frequency fluctuations is then $S_{ff}(f) = |H_f^{\tilde{F}(z)=0}(f)|^2 S_{vv}(f) + |H_f^{\tilde{V}(z)=0}(f)|^2 S_{ff}(f)$, assuming we can independently sum the contributions from the sampling noise and the qubit frequency fluctuations, shown in Fig. S1d for the same parameters as used in Fig. 1d in the main text. Quite remarkably, this analysis very closely reproduces the simulation of the qubit frequency fluctuation spectral density shown with red in Fig. 1d.

C. Spectral density of flux noise

The measured coefficients $k_{E/R}$ can be connected to the spectral density of $1/f$ flux noise, $S_{\Phi\Phi}(f) = A_\Phi/|2\pi f|$, as

$$\sqrt{A_\Phi} = \frac{k_{E/R}}{2\pi\sqrt{\eta_{E/R}}}, \quad (\text{S15})$$

where the labels E or R refer either to echo or Ramsey sequence, and $\eta_{E/R}$ is a scaling parameter which depends on the bandwidth of the noise to which the used pulse sequence is sensitive, $\eta_E = \ln 2$, and $\eta_R = \ln \frac{f_u}{2\pi f_l} \approx 13$ [27]. Here, we take the upper cutoff frequency $f_u = 100 \text{ kHz} \sim 1/T_2$ and the lower cutoff frequency $f_l = 40 \text{ mHz}$ corresponding to the inverse of the total duration of the Ramsey experiment. By substituting the measured values of k to the above formula, we infer $\sqrt{A_\Phi} = 2.8 \mu\Phi_0$ without the feedback. With the feedback activated, the flux noise spectral density no longer follows $1/f$ law due to the suppression of low frequency noise, but for comparison we can still calculate an effective flux noise amplitude using Eq. (S15), which yields $\sqrt{A_\Phi} = 2.4 \mu\Phi_0$. When measured using the echo sequence we get $\sqrt{A_\Phi} = 3.3 \mu\Phi_0$. Ideally, the flux noise amplitude inferred from the Ramsey experiment without the feedback should yield the same value as the flux noise amplitude calculated from the echo experiment, but we attribute the discrepancy to the deviation of the noise spectrum from the ideal $1/f$ spectrum, as observed earlier in Fig. 1b. The measured flux noise amplitude is consistent with the earlier systematic study we performed for flux noise amplitudes of SQUID loops of different sizes [10].

D. Experimental setup and the hardware implementation

Fig. S2 shows the hardware setup used in the experiment. The qubit XY control and readout pulses are created by a Keysight PXI arbitrary waveform generator. The in-phase and quadrature pulses are up-converted to the qubit and the resonator frequencies using a R&S SGMA RF source, which has a built-in IQ-mixer used for single-sideband modulation. The signals are attenuated to mitigate thermal noise from room-temperature, and sent to the qubit installed in a Leiden Cryogenics dilution refrigerator. After interacting with the readout resonator, the readout signal is amplified by a traveling wave parametric amplifier (TWPA), which is driven by a pump tone. The TWPA is followed by a chain of conventional amplifiers and the signal is digitized at room-temperature using a Keysight PXI digitizer.

The qubit flux bias is controlled by two channels of another Keysight PXI AWG. The first channel is used to set the operating point for the qubit, whereas the second channel is controlled by the feedback loop. The feedback channel is heavily attenuated in order to use the full voltage bandwidth of the AWG to reduce the discretization noise.

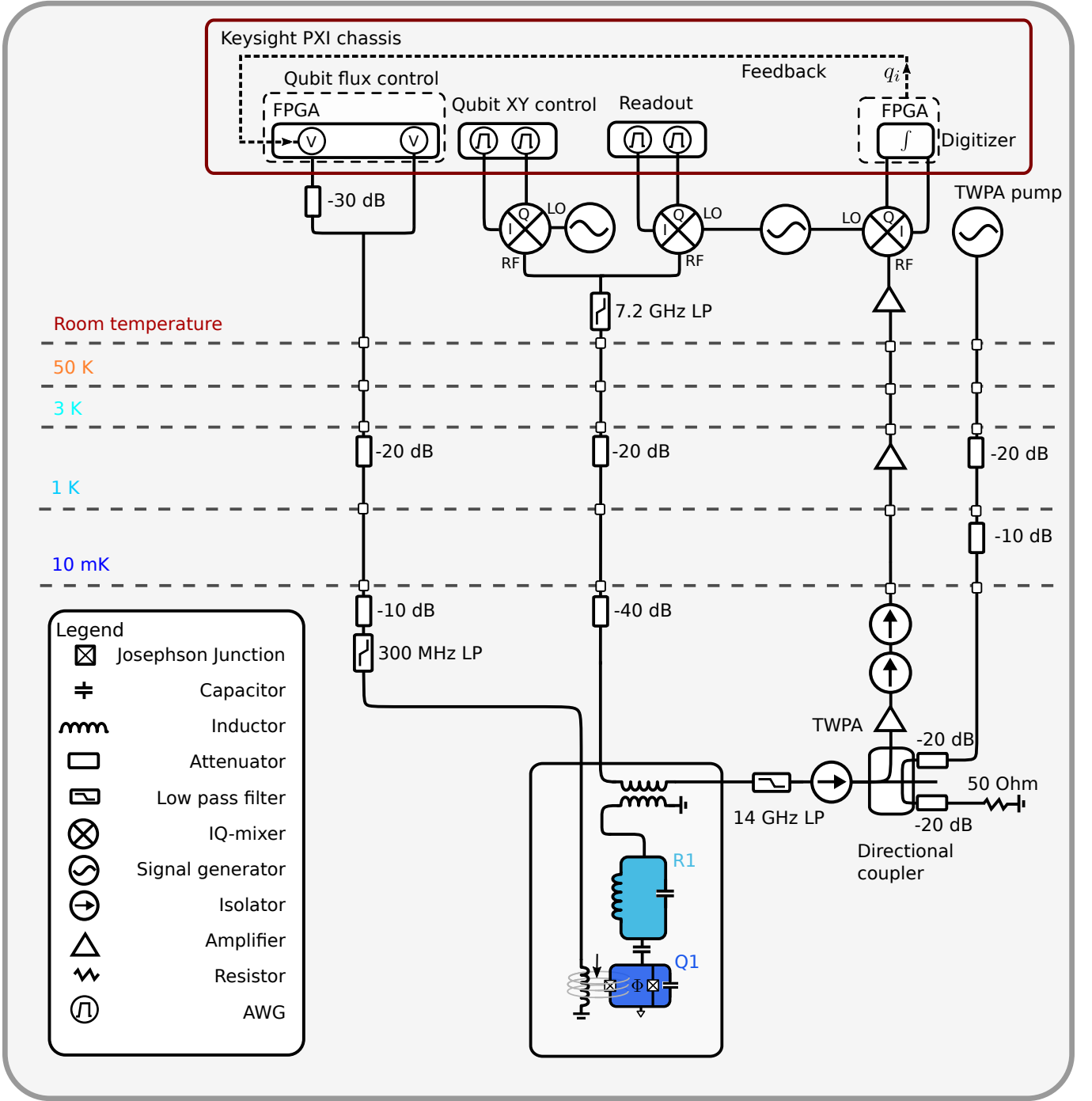


FIG. S2. The experimental setup.

The feedback loop is formed by the readout digitizer and the qubit flux control AWG. The on-board FPGA of the digitizer is used to digitally demodulate and integrate the readout signal and then use a threshold discriminator to assign the qubit state q_i to either 0 or 1, see Fig. S3 for the block diagram of the FPGA operation. The discriminated states are transferred to the AWG for the calculation of the feedback signal.

First we perform the virtual qubit state reset by flipping the discriminated state q_i if the previous discriminated state was excited state. This is equivalent to $q_i \rightarrow \text{XOR}(q_i, q_{i-1})$. In the next step, the q_i are used to calculate the estimate for the qubit state $s_i = N\hat{p}_1 = \sum_{j=i-N+1}^i q_j = s_{i-1} - q_{i-N+1} + q_i$. The value of the buffer sum s is used as an index for a lookup table which contains the binary representation of the voltages corresponding to each of the possible $N + 1$ values for s_i . In the last step, the voltage values are fed to an accumulator, which value is updated every N_S

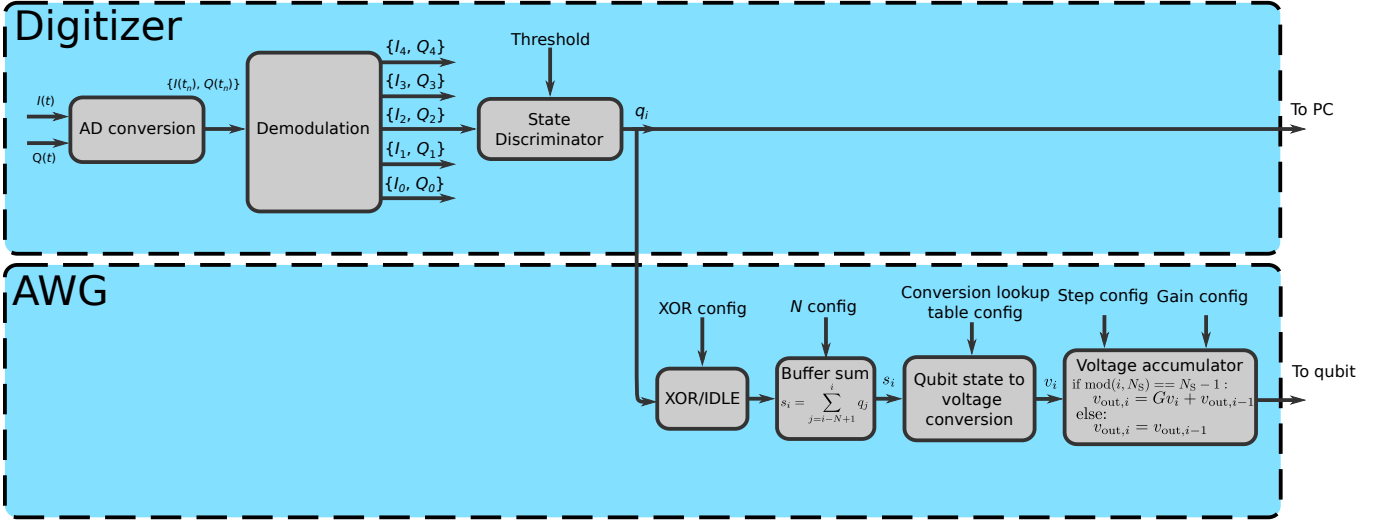


FIG. S3. The block diagram of the two FPGAs performing the feedback. The FGPA in the digitizer discriminates the state, and forwards the information to the FPGA which controls the AWG.

steps. We set $N_S = N$ for the measurement of the qubit frequency fluctuation spectral density, and $N_S = N + 1$ for the interleaved operation.

E. Coherence limit in randomized benchmarking

The limit imposed on the gate fidelity by decoherence has been studied for example in [30, 37]. The error probability per gate due to decoherence depends on the gate time and the coherence times as

$$\epsilon = \frac{t_{\text{gate}}}{3T_1} + \frac{t_{\text{gate}}}{3T_{\phi 1}} + \frac{1}{3} \left(\frac{t_{\text{gate}}}{T_{\phi 2}} \right)^2, \quad (\text{S16})$$

where T_1 is the energy-relaxation rate of the qubit, $T_{\phi 1}$ is the exponential part of the pure dephasing time, and $T_{\phi 2}$ is the Gaussian part of the pure dephasing time. In the experiment, we have $t_{\text{gate}} = 40$ ns, which consists of 30 ns long cosine-shaped envelope and 10 ns delay between the pulses. The T_1 times of our qubit were between 26 μ s and 40 μ s, depending on the bias point used in the experiment. Using Eq. (S16), we calculate ϵ at all the 11 bias points used in the experiment, yielding values in the range of 3×10^{-4} to 5×10^{-4} , which are shown with black dots in Fig. 4c in the main text. The gate errors due to the Gaussian dephasing $\frac{1}{3} \left(\frac{t_{\text{gate}}}{T_{\phi 2}} \right)^2 < 0.33 \times 10^{-4}$ contribute to the total error rate significantly less than the energy-relaxation rate, even at the most sensitive bias point where $T_{\phi 2} \approx 4$ μ s. Feedback improved the dephasing time to $T_{\phi 2} \approx 5$ μ s, which according to the estimate would reduce the Gaussian dephasing induced error rate to $\sim 0.2 \times 10^{-4}$. However, the measured decrease in gate errors was significantly higher, from $(8.5 \pm 2.1) \times 10^{-4}$ to $(5.9 \pm 0.7) \times 10^{-4}$. We attribute the higher efficiency of the feedback to its ability to correct slow frequency fluctuations of the qubit, not captured by a single T_2 experiment.